INTERNATIONAL JOURNAL FOR NUMERICAL METHODS IN FLUIDS
*Int. J. Numer. Meth. Fluids* 2008; **57**:1–12
Published online 20 September 2007 in Wiley InterScience (www.interscience.wiley.com). DOI: 10.1002/fld.1609

# Adaptive-quadrature fluctuation-splitting schemes for the Euler equations

Hiroaki Nishikawa*, †

*W. M. Keck Foundation Laboratory for Computational Fluid Dynamics, Department of Aerospace Engineering, University of Michigan, FXB Building, 1320 Beal Avenue, Ann Arbor, MI 48109-2140, U.S.A.*

SUMMARY

In this paper, we present fluctuation-splitting schemes that can capture an isolated shock over a suitably oriented single triangular element and also recognize a rarefaction. A particular focus is on the evaluation of the fluctuation (or the cell residual): a one-parameter-family quadrature rule is employed to evaluate the fluctuation, which endows the fluctuation with a wave recognition capability. The parameter value is chosen based on the nature of the nonlinear wave passing through the element, and then the resulting fluctuation is distributed to the nodes. This strategy, combined with various distribution schemes, defines a family of adaptive-quadrature fluctuation-splitting schemes. The results demonstrate the superior ability of the new schemes in handling nonlinear waves compared with standard fluctuation-splitting schemes that cannot capture shocks over a single element and also admits nonphysical shocks unless some kind of entropy fix is incorporated. Copyright © 2007 John Wiley & Sons, Ltd.

Received 18 December 2006; Revised 19 July 2007; Accepted 21 July 2007

KEY WORDS: adaptive quadrature; shock-capturing; entropy fix; fluctuation-splitting; residual distribution; feature detection

## 1. INTRODUCTION

Fluctuation-splitting (or residual-distribution) schemes are multidimensional upwinding schemes that have been developed mainly for unstructured triangular/tetrahedral meshes [1–7]. These schemes are based on cell residual (fluctuation) with variables stored at nodes and consist of two steps: compute the flux balance (fluctuation/residual) over an element; distribute it to the nodes of the element to bring changes to the nodal variables. Note that both steps are based on

*Correspondence to: Hiroaki Nishikawa, National Institute of Aerospace, 100 Exploration Way, Hampton, VA 23666-6147, U.S.A.
†E-mail: hiro@nianet.org

Contract/grant sponsor: Space Vehicle Technology Institute; contract/grant number: NCC3-989
Contract/grant sponsor: Department of Defense

complete elements, not on lower-dimensional components such as faces or edges (as in the finite-volume methods). This element-wise operation enables multidimensional physics to be directly taken into account, and this is one of the advantages of the fluctuation-splitting schemes over the finite-volume schemes.

Despite many superior features over the conventional finite-volume schemes, however, existing fluctuation-splitting schemes cannot capture a shock over a single element and also admits nonphysical shocks. A form of entropy fix has been reported by Sermeus and Deconinck [8]. Their method is based on modifying the wave speeds in the distribution matrices. This generalizes the one-dimensional entropy fix of Harten and Hyman [9]. In this work, we take a different approach and develop a method that can compute entropy-satisfying expansions as well as capture a shock over a single element, focusing on the evaluation of the fluctuation. In the development of the fluctuation-splitting schemes, the effort has been put mainly in the development of the distribution coefficients while the fluctuation itself has been evaluated exclusively with the conservative linearization [10]. Some recent works focus on more general quadrature rules to evaluate the fluctuation, in order to make it possible to apply the fluctuation-splitting schemes to general systems of equations for which the exact linearization may not be possible [11], or to achieve higher order accuracy [5, 12]. In [13], the authors also use the term 'adaptive quadrature' but with a different sense. They increase the accuracy of the numerical quadrature in nonsmooth regions to restore conservation to a nonconservative method. Our quadrature is always second order and conservative but adapts to make a correct distinction between shocks and rarefactions. This paper explores yet another possibility of using quadrature formulas for fluctuations to control the wave recognition property of the fluctuation-splitting schemes. For the Euler equations, a one-parameter family of quadrature rules is employed to evaluate the fluctuation. The resulting fluctuation is given flexibility to handle different kinds of flow features by the freedom to choose the parameter. The parameter value is chosen based on the nature of the nonlinear wave that is present inside the element. In order to detect such waves (shocks or rarefactions), a multidimensional way of detecting nonlinear waves is also devised.

Section 2 gives an overview of the fluctuation-splitting schemes with a particular emphasis on those that can distribute the fluctuation evaluated by a general quadrature rule. Section 3 describes the quadrature rule for the fluctuation and its properties. Section 4 discusses a way to detect shocks/expansions and to assign the parameter. Section 5 shows results. Section 6 concludes the paper.

## 2. FLUCTUATION-SPLITTING SCHEMES

We consider solving sets of conservation laws of the form

$$\mathbf{u}_t + \partial_x \mathbf{f} + \partial_y \mathbf{g} = 0 \tag{1}$$

where $\mathbf{u}$ is a vector of conservative variables, in the domain divided into a set of triangles $\{T\}$. In the fluctuation-splitting schemes, the first step is to compute the fluctuation $\mathbf{\Phi}^T$ for all triangles $T \in \{T\}$:

$$\mathbf{\Phi}^T = -\int_T \mathbf{u}_t \, \mathrm{d}V = \int_T (\partial_x \mathbf{f} + \partial_y \mathbf{g}) \, \mathrm{d}V \tag{2}$$

which is evaluated by a certain quadrature rule. This is the focus of this paper and will be discussed in detail in the next section. The second step is to distribute the fluctuation, in a way



DOI: 10.1002/fld

that reflects multidimensional physics, to the nodes to suggest changes in the nodal variables. This results in the following update formula at node $j$:

$$\mathbf{u}_j^{n+1} = \mathbf{u}_j^n - \frac{\Delta t}{V_j} \sum_{T \in \{T_j\}} \mathbf{\Phi}_i^T \tag{3}$$

where

$$\mathbf{\Phi}_i^T = \mathscr{B}_j^T \mathbf{\Phi}^T \tag{4}$$

and $\{T_j\}$ is a set of triangles that share the node $j$, $\Delta t = t^{n+1} - t^n$ is a global time step, $V_j$ is the measure of the median dual control volume, and $\mathscr{B}_j^T$ is the distribution matrix that assigns the fraction of the fluctuation sent to node $j$ within triangle $T$. We consider only conservative schemes characterized by

$$\sum_j \mathscr{B}_j^T = I \tag{5}$$

where $I$ is the identity matrix. Various such distribution matrices are available. They are all based on the so-called inflow matrix and its characteristic decomposition is defined by

$$\mathbf{K}_i = \tfrac{1}{2}(\mathbf{A}, \mathbf{B}) \cdot \mathbf{n}_i, \quad \mathbf{K}_i^{\pm} = \mathbf{R}_i \mathbf{\Lambda}_i^{\pm} (\mathbf{R}_i)^{-1} \tag{6}$$

where $\mathbf{A} = \frac{\partial \mathbf{f}}{\partial \mathbf{u}}$, $\mathbf{B} = \frac{\partial \mathbf{g}}{\partial \mathbf{u}}$, $\mathbf{n}_i = (n_i^x, n_i^y)$ is the scaled inward normal vector opposite to the node $i$, the columns of $\mathbf{R}_i$ are the right eigenvectors of $\mathbf{K}_i$, and $\mathbf{\Lambda}$ is the corresponding diagonal matrix of the eigenvalues. In this work, we use the nonlinear matrix $N$-scheme of Csik *et al.* [11]

$$\mathbf{\Phi}_i^T = \mathbf{K}_i^+ (\mathbf{u}_i - \mathbf{u}_{in}) \tag{7}$$

where

$$\mathbf{u}_{in} = -\left( \sum_i \mathbf{K}_i^- \right)^{-1} \left( \sum_i \mathbf{K}_i^+ \mathbf{u}_i - \mathbf{\Phi}^T \right) \tag{8}$$

and also the matrix LDA scheme,

$$\mathscr{B}_j^T = \mathbf{K}_j^+ \left( \sum_i \mathbf{K}_i^+ \right)^{-1} \tag{9}$$

The former is used when the monotonicity is important while the latter is used when the linearity-preserving property is important. The primary reason for these, however, is that both of these schemes can distribute the fluctuation independently of how it is evaluated. We need this property because we are going to compute the fluctuation in an adaptive manner.

Note that there exist typically twice as many triangles as nodes in a triangular mesh, and hence there are twice as many fluctuations as nodal solutions. This results in a highly overdetermined problem, and, therefore, the fluctuation $\mathbf{\Phi}^T$ cannot be made to vanish everywhere. To equalize the number of unknowns and the number of equations, we define a nodal residual at every node by taking a weighted average of the fluctuations over the triangles that share the node. However, it is reasonable to assume that the fluctuations are small at convergence, and usually they are. In this sense, the distribution step may be thought of as minimizing the fluctuations by rendering



DOI: 10.1002/fld

appropriate changes to the nodal variables. In fact, this is precisely the case for the least-squares scheme [14] in which $\mathscr{B}_j^T$ is the negative gradient of the fluctuation with respect to the nodal variables, and this also applies to the LDA scheme that is known to be a variant of the least-squares scheme. On the basis of this particular viewpoint, in this work, we design the fluctuation-splitting schemes in terms of how the fluctuation is defined rather than how to distribute it.

## 3. QUADRATURE FORMULA

We consider conservation laws for which each component of the fluxes is a bilinear function of the components of a certain set of variables $\mathbf{w}$

$$\mathbf{f}(\mathbf{w}) = \mathbf{w}^{\mathrm{t}}\mathbf{C}\mathbf{w}, \quad \mathbf{g}(\mathbf{w}) = \mathbf{w}^{\mathrm{t}}\mathbf{D}\mathbf{w} \tag{10}$$

where $\mathbf{C}$ and $\mathbf{D}$ are constant symmetric third-order tensors, and the superscript t denotes the transpose. This structure includes the Euler equations of compressible inviscid flow if $\mathbf{w}$ is taken to be Roe's parameter vector [15]. Note that we have

$$\mathbf{A}_w(\mathbf{w}) = \frac{\partial \mathbf{f}}{\partial \mathbf{w}}(\mathbf{w}) = 2\mathbf{w}^{\mathrm{t}}\mathbf{C} \tag{11}$$

$$\mathbf{B}_w(\mathbf{w}) = \frac{\partial \mathbf{g}}{\partial \mathbf{w}}(\mathbf{w}) = 2\mathbf{w}^{\mathrm{t}}\mathbf{D} \tag{12}$$

Fluctuation over a triangle defined by the vertices 1–2–3 is

$$\mathbf{\Phi}_{123} = \iint_{123} [\partial_x \mathbf{f}(\mathbf{w}) + \partial_y \mathbf{g}(\mathbf{w})]\,\mathrm{d}x\,\mathrm{d}y \tag{13}$$

$$= \oint_{123} [\mathbf{f}(\mathbf{w})\,\mathrm{d}y - \mathbf{g}(\mathbf{w})\,\mathrm{d}x] \tag{14}$$

Along each edge, there is a class of simple quadrature formulas [16] defined by

$$\begin{aligned}\mathbf{F}_{12} &= \int_1^2 \mathbf{f}(\mathbf{w})\,\mathrm{d}y = \int_1^2 \mathbf{w}^{\mathrm{t}}\mathbf{C}\mathbf{w}\,\mathrm{d}y \\ &= (y_2 - y_1)\left[\mathbf{w}_1^{\mathrm{t}}\mathbf{C}\mathbf{w}_2 + \frac{\alpha}{2}(\mathbf{w}_2 - \mathbf{w}_1)^{\mathrm{t}}\mathbf{C}(\mathbf{w}_2 - \mathbf{w}_1)\right]\end{aligned} \tag{15}$$

where $\alpha$ is a parameter to be assigned. Clearly, the formula is second-order accurate for any $\alpha$. If we assume, although we do not have to, that the same value is assigned to $\alpha$ for all edges, then by collecting contributions from all edges, and arranging, we arrive at

$$\begin{aligned}\mathbf{\Phi}_{123} = {} & \frac{1}{2}\sum_i [\mathbf{A}_w(\tilde{\mathbf{w}}_\alpha) n_i^x + \mathbf{B}_w(\tilde{\mathbf{w}}_\alpha) n_i^y]\mathbf{w}_i \\ & - \frac{\beta}{2}[(\mathbf{A}_w(\mathbf{w}_3) n_2^x + \mathbf{B}_w(\mathbf{w}_3) n_2^y)\mathbf{w}_1 \\ & + (\mathbf{A}_w(\mathbf{w}_1) n_3^x + \mathbf{B}_w(\mathbf{w}_1) n_3^y)\mathbf{w}_2 \\ & + (\mathbf{A}_w(\mathbf{w}_2) n_1^x + \mathbf{B}_w(\mathbf{w}_2) n_1^y)\mathbf{w}_3]\end{aligned} \tag{16}$$



DOI: 10.1002/fld

where

$$\tilde{\mathbf{w}}_\alpha = \frac{\alpha}{2}(\mathbf{w}_1+\mathbf{w}_2+\mathbf{w}_3), \quad \beta = \frac{3}{2}\left(\frac{2}{3}-\alpha\right) \tag{17}$$

It follows immediately from this that the choice $\alpha=\frac{2}{3}$ corresponds to the so-called conservative linearization [10], which has been almost exclusively the choice of previous investigations.

Suppose that two of the nodes of a triangle happen to be in the same state, say $\mathbf{w}_1=\mathbf{w}_2=\mathbf{w}_c$ (see Figure 1). Then, we have

$$\begin{aligned}\boldsymbol{\Phi}_{123} = {} & (y_3-y_2)\left[\mathbf{w}_2^{\mathrm{t}}\mathbf{C}\mathbf{w}_3+\frac{\alpha}{2}(\mathbf{w}_3-\mathbf{w}_2)^{\mathrm{t}}\mathbf{C}(\mathbf{w}_3-\mathbf{w}_2)\right]\\ & +(y_1-y_3)\left[\mathbf{w}_1^{\mathrm{t}}\mathbf{C}\mathbf{w}_3+\frac{\alpha}{2}(\mathbf{w}_1-\mathbf{w}_3)^{\mathrm{t}}\mathbf{C}(\mathbf{w}_1-\mathbf{w}_3)\right]\\ & +(y_2-y_1)\mathbf{w}_1^{\mathrm{t}}\mathbf{C}\mathbf{w}_2\\ & -(x_3-x_2)\left[\mathbf{w}_2^{\mathrm{t}}\mathbf{D}\mathbf{w}_3+\frac{\alpha}{2}(\mathbf{w}_3-\mathbf{w}_2)^{\mathrm{t}}\mathbf{C}(\mathbf{w}_3-\mathbf{w}_2)\right]\\ & -(x_1-x_3)\left[\mathbf{w}_1^{\mathrm{t}}\mathbf{D}\mathbf{w}_3+\frac{\alpha}{2}(\mathbf{w}_1-\mathbf{w}_3)^{\mathrm{t}}\mathbf{D}(\mathbf{w}_1-\mathbf{w}_3)\right]\\ & -(x_2-x_1)\mathbf{w}_1^{\mathrm{t}}\mathbf{D}\mathbf{w}_2\end{aligned} \tag{18}$$

Note that the terms proportional to $\alpha$ have identically vanished along the edge 1–2, i.e. the fluctuation is independent of $\alpha$ for the edge along which the solution value is constant. The fluctuation further simplifies to

$$\boldsymbol{\Phi}_{123} = \overline{\mathbf{w}}_\alpha^{\mathrm{t}}[\Delta y\mathbf{C}-\Delta x\mathbf{D}](\mathbf{w}_c-\mathbf{w}_3) \tag{19}$$

where $\Delta() = ()_2-()_1$, and

$$\overline{\mathbf{w}}_\alpha = \frac{2-\alpha}{2}\mathbf{w}_c+\frac{\alpha}{2}\mathbf{w}_3 \tag{20}$$

Now, with $\alpha=1$, this discretization becomes precisely the Rankine–Hugoniot relation, with $S$ being the slope of the shock,

$$S[\mathbf{f}(\mathbf{w}_c)-\mathbf{f}(\mathbf{w}_3)]-[\mathbf{g}(\mathbf{w}_c)-\mathbf{g}(\mathbf{w}_3)] = \left(\frac{\mathbf{w}_c+\mathbf{w}_3}{2}\right)^{\mathrm{t}}(S\mathbf{C}-\mathbf{D})(\mathbf{w}_c-\mathbf{w}_3)=0 \tag{21}$$

provided the shock is parallel to the edge 1–2, i.e. $S=\Delta y/\Delta x$. This was originally shown in [16], but it was not explicitly stated that this property is independent of $\alpha$ for the edge parallel to the shock. This result shows that a shockwave can be spanned by a single element, and therefore captured exactly, only if $\alpha=1$. It also shows that the capturing element can be arbitrarily narrow, so that the shock can be captured with arbitrarily high resolution. Of course, these properties are not fully exploitable unless the mesh is made adaptive, and this is an aspect on which we are not yet ready to report. Although Equation (21) coincides with the Rankine–Hugoniot condition when $\alpha=1$, it does not distinguish the direction of the jump and hence admits expansion shocks. However, the nonphysical shocks can be avoided simply by taking a different value of $\alpha$. This parameter $\alpha$ is in fact closely related to the entropy production. A one-dimensional analysis for



DOI: 10.1002/fld

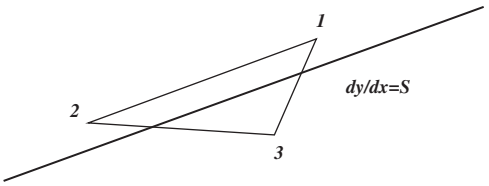


Figure 1. A shock passing through an element.

Burgers' equation shows that the entropy function is conserved with $\alpha=\frac{2}{3}$ and reduced with $\alpha<\frac{2}{3}$, thus ensuring physical solutions [16, 17].

## 4. ADAPTIVE QUADRATURE

To choose the value of $\alpha$ for a particular element, we need to know if the element is in a shock or in a rarefaction or away from such nonlinear waves. For this purpose, we use the divergence of the *steady*-characteristic speeds

$$\int_T \operatorname{div}\boldsymbol{\lambda}^k \,\mathrm{d}x\,\mathrm{d}y=\frac{1}{2}\sum_i \boldsymbol{\lambda}_i^k\cdot\mathbf{n}_i \tag{22}$$

where $\boldsymbol{\lambda}^k$ has been assumed to vary linearly over the element and $\boldsymbol{\lambda}_i^k$ is the $k$th steady-characteristic speed vector evaluated at node $i$. For the sake of convenience, in this work, we define the following:

$$\Delta_k=\frac{\sum_i \boldsymbol{\lambda}_i^k\cdot\mathbf{n}_i}{\sum_i |\boldsymbol{\lambda}_i^k||\mathbf{n}_i|} \tag{23}$$

in which the quantity in the denominator has been introduced to normalize $\Delta_k$ such that

$$-1\leqslant\Delta_k\leqslant 1 \tag{24}$$

We know that a shock is present if this quantity is negative (converging characteristic field) and a rarefaction presents if positive (diverging characteristic field). This leads us to dividing the range into three parts:

$$\alpha=\begin{cases}1, & -1\leqslant\Delta_k\leqslant-\delta\\ \frac{2}{3}, & -\delta<\Delta_k<\delta\\ 0, & \delta\leqslant\Delta_k\leqslant 1\end{cases} \tag{25}$$

We experimentally found that it worked well with $\delta\approx 10^{-3}$.

For the Euler equations, there are two possible nonlinear waves in supersonic flows. Their characteristic speeds are given by

$$\boldsymbol{\lambda}^1=(u\beta-v,\, v\beta+u) \tag{26}$$

$$\boldsymbol{\lambda}^2=(u\beta+v,\, v\beta-u) \tag{27}$$



DOI: 10.1002/fld

where $\beta=\sqrt{M^2-1}$ [18]. Note that

$$\operatorname{div}\boldsymbol{\lambda}^1=\operatorname{div}(\beta\mathbf{q})-\omega \tag{28}$$

$$\operatorname{div}\boldsymbol{\lambda}^2=\operatorname{div}(\beta\mathbf{q})+\omega \tag{29}$$

where $\mathbf{q}=(u,v)$ and $\omega=\partial_x v-\partial_y u$. This means that we detect and distinguish waves using a combination of the divergence and the vorticity of the flow field. Note also that we have

$$(\operatorname{div}\boldsymbol{\lambda}^1)^2+(\operatorname{div}\boldsymbol{\lambda}^2)^2=[\operatorname{div}(\beta\mathbf{q})]^2+\omega^2 \tag{30}$$

This provides an interesting link between physical quantities and the existence of nonlinear waves.

In actual implementation, we first look at the Mach number at three vertices. We take $\alpha=\frac{2}{3}$ if all of the nodes of an element are in a subsonic flow for which the acoustic system is elliptic and there exist no steady characteristics. Also, we immediately take $\alpha=1$ for the elements with both subsonic and supersonic nodes as it indicates the presence of a strong shock running across the element. For fully supersonic elements, we compute $\Delta_k$ for $k=1,2$, take the larger of the two in magnitude (the dominant wave), and then use (25) to determine the value of $\alpha$ for the element.

The resulting method will not be conservative if $\alpha$ is assigned element-wise because line integrals do not cancel over an edge shared by two triangles with different $\alpha$. This can be fixed by unifying the value of $\alpha$ over such an edge whenever the line integral would be evaluated with different $\alpha$ in the adjacent elements. In this work, we set $\alpha=\frac{2}{3}$ if either of the two $\alpha$'s is $\frac{2}{3}$, and set $\alpha=1$ if either of the two $\alpha$'s is 1.

## 5. RESULTS

For all results, the distribution matrices were evaluated as the arithmetic average of the parameter vector over a triangle. For those with the adaptive quadrature, the parameter $\alpha$ was determined by criterion (25) with $\delta=3.0\times10^{-3}$. All computations were performed with double precision.

### *5.1. Supersonic flow over a triangular bump*

The first test case is a supersonic flow over a triangular bump at Mach number of 1.69. The grid is a regular triangular grid of size $100\times50$ nodes (see Figure 2). All cases here were computed with the nonlinear matrix $N$-scheme (7). Figure 3(a)–(c) shows the Mach contours for cases with $\alpha=1$, $\alpha=\frac{2}{3}$, $\alpha=0$, respectively, for all triangles. It is clear from these that the choice of $\alpha=1$ results in an expansion shock, $\alpha=\frac{2}{3}$ still suffers from an expansion shock although weaker, and $\alpha=0$ produces a correct expansion fan. See also Figure 4(a)–(c) shows the plots of Mach number along a line passing over the waves at $y=0.65$, sampled from the corresponding results in Figure 3. Results with the adaptive choice of $\alpha$ are shown in Figures 3(d) and 4(d). As expected, we see that the expansion fan is as cleanly computed as the one with $\alpha=0$ everywhere. We point out that in this adaptive case the residuals do not converge to machine zero, stagnating at the values of order $10^{-7}$ in the $L_1$ norm which is equivalent to three orders of magnitude reduction based on the initial residuals, i.e. practically converged. Finally, we remark that the shock/expansion detection mechanism works very well, accurately identifying elements in the shocks and the rarefaction as shown in Figure 5.



DOI: 10.1002/fld

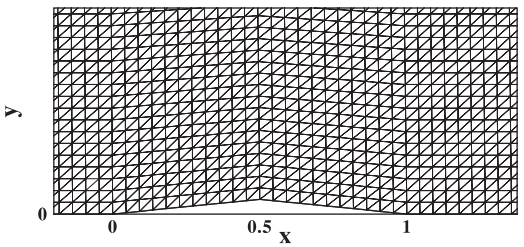


Figure 2. A blow-up of the grid used for the first test case.

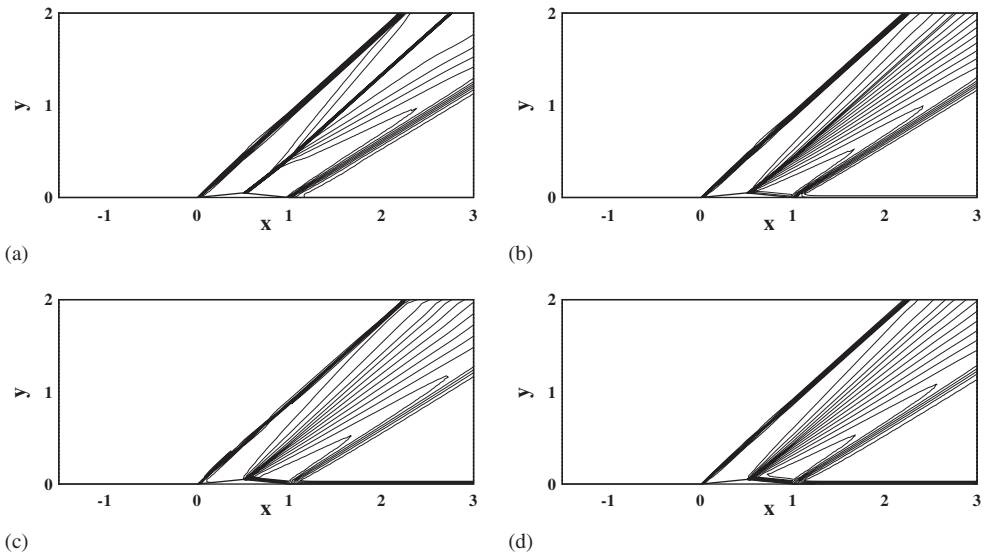


Figure 3. Results by the nonlinear N-Scheme with various types of fluctuations: (a) $\alpha=1$; (b) $\alpha=\frac{2}{3}$; (c) $\alpha=0$; and (d) $\alpha$ adaptively assigned.

### 5.2. *Shock reflection*

The second test case is a shock-reflection problem. The boundary conditions are

$$\begin{bmatrix} \rho \\ M\cos\theta \\ M\sin\theta \\ p \end{bmatrix} = \begin{bmatrix} 1 \\ 1.878327025 \\ 0 \\ 1 \end{bmatrix} \tag{31}$$



DOI: 10.1002/fld

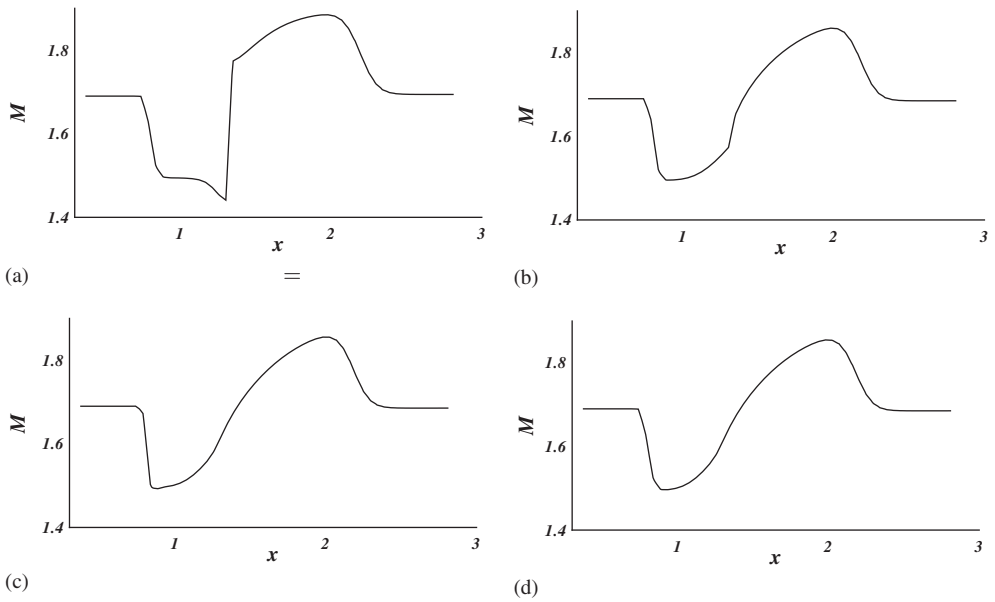


Figure 4. Plots of Mach number along a line at $y=0.65$: (a) $\alpha=1$; (b) $\alpha=\frac{2}{3}$; (c) $\alpha=0$; and (d) $\alpha$ adaptively assigned.

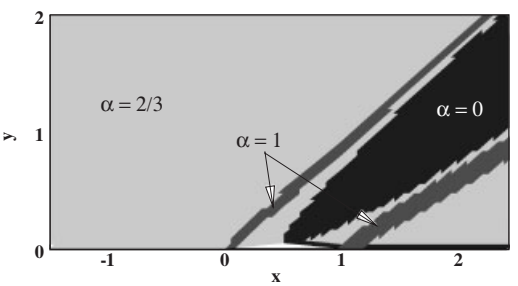


Figure 5. Element-wise distribution of $\alpha$ over the domain.

for upstream, and

$$\begin{bmatrix} \rho \\ M\cos\theta \\ M\sin\theta \\ p \end{bmatrix} = \begin{bmatrix} 1.44089676 \\ 1.52567142\cos 10^\circ \\ 1.52567142\sin 10^\circ \\ 1.67694833 \end{bmatrix} \tag{32}$$

for the upper boundary. A wall boundary condition is imposed on the bottom boundary. The grid, shown in Figure 6, was generated such that edges are perfectly aligned with both an incoming shock and its reflection. For this problem, we employed the LDA scheme (7). Two approaches are



DOI: 10.1002/fld

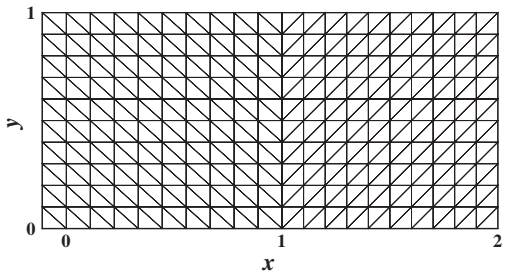


Figure 6. Grid for the shock-reflection test case. $21 \times 11$ nodes.

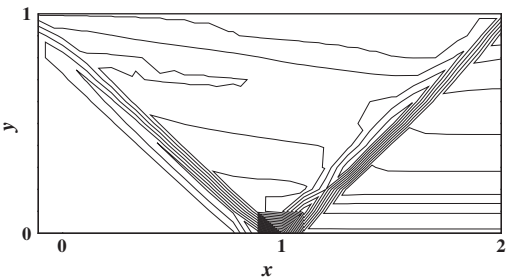


Figure 7. Entropy contours. The LDA-Scheme with $\alpha = \frac{2}{3}$.

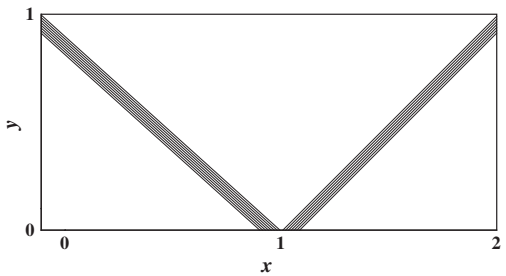


Figure 8. Entropy contours. The LDA-Scheme with adaptive $\alpha$.

compared here: the LDA with $\alpha = \frac{2}{3}$, the LDA with adaptive $\alpha$. We start from the common initial solution: the inflow condition is specified everywhere. Figure 7 shows the entropy contours for the LDA scheme with the conservative linearization ($\alpha = \frac{2}{3}$). The solution is not particularly clean, but this is not surprising for nonmonotone schemes such as the LDA. Figure 8 shows the entropy contours obtained by the same LDA scheme but with $\alpha$ adaptively assigned for the fluctuation. The solution is virtually exact with no spurious entropy whatsoever. As seen in Figure 9 where the value of $\alpha$ is plotted element-wise, the elements in the shocks have been perfectly detected, and a suitable value of $\alpha(=1)$ is assigned. And because these elements have a side parallel to the shock, their fluctuations completely vanish, satisfying the Rankine–Hugoniot relation.



DOI: 10.1002/fld

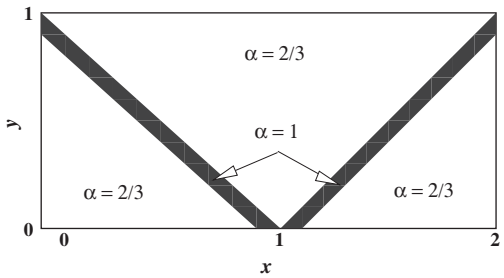


Figure 9. Element-wise distribution of $\alpha$ over the domain.

## 6. CONCLUDING REMARKS

This paper has shown that the fluctuation-splitting schemes can be designed to recognize shocks over a single element as well as to avoid nonphysical shocks by evaluating the fluctuation in an adaptive manner. Results show significant improvement over the conventional schemes. Also, the nonlinear wave detection algorithm has shown to work so well that it could be used alone for other purposes, for example, to identify regions for grid refinement.

In this work, we first assigned the parameter $\alpha$ for all elements and then computed the fluctuations. These two processes may be combined into a single-loop process to improve the efficiency. It would also be possible to assign $\alpha$ edge-wise rather than element-wise because $\alpha$ does not have to be the same within the element and it would eliminate the need to fix the conflicting $\alpha$ on edges for conservation.

For shock capturing, the method would work best with an adaptive grid method because the single-element shock capturing is possible only when one of the edges is aligned with the shock. One strategy would be to generate shock-aligned elements by moving the nodes as well as computing the solutions so as to minimize the fluctuations in the least-squares norm. In fact, this has already been demonstrated for Burgers' equation in [16]. We remark that we can apply such grid movement only for limited regions by taking advantage of the excellent capability of the wave detection algorithm.

ACKNOWLEDGEMENTS

This work has been sponsored by the Space Vehicle Technology Institute, under grant NCC3-989, one of the NASA University Institutes, with joint sponsorship from the Department of Defense. I would like to thank Professor P. L. Roe for his comments.

REFERENCES

1. Crumpton PI, MacKenzie JA, Morton KW. Cell vertex algorithms for the compressible Navier–Stokes equations. *Journal of Computational Physics* 1993; **109**:1–15.
2. Ni R-H. A multiple-grid scheme for solving the Euler equations. *AIAA Journal* 1982; **20**(11):1565–1571.
3. Abgrall R. Toward the ultimate conservative scheme: following the quest. *Journal of Computational Physics* 2001; **167**:277–315.
4. Sermeus K, Deconinck H. Solution of steady Euler and Navier–Stokes equations using residual distribution schemes. *Thirty-Third Computational Fluid Dynamics—Novel Methods for Solving Convection Dominated Systems*, VKI Lecture Series, von Karman Institute for Fluid Dynamics, Belgium, 2003.



DOI: 10.1002/fld

5. Caraeni D, Fuchs L. Compact third-order multidimensional upwind scheme for Navier–Stokes simulations. *Theoretical and Computational Fluid Dynamics* 2002; **15**:373–401.
6. Hubbard ME, Laird AL. Achieving high-order fluctuation splitting schemes by extending the stencil. *Computers and Fluids* 2005; **34**:443–459.
7. Rossiello G, De Palma P, Pascazio G, Napolitano M. Third-order-accurate fluctuation-splitting schemes for unsteady hyperbolic problems. *Journal of Computational Physics* 2007; **222**:332–352.
8. Sermeus K, Deconinck H. An entropy fix for multi-dimensional upwind residual distribution schemes. *Computers and Fluids* 2005; **34**:617–640.
9. Harten A, Hyman JM. Self-adjusting grid methods for one-dimensional hyperbolic conservation laws. *Journal of Computational Physics* 1983; **50**:235–269.
10. Deconinck H, Roe PL, Struijs R. A multi-dimensional generalization of Roe's flux difference splitter for the Euler equations. *Computers and Fluids* 1993; **22**:215–222.
11. Csik A, Ricchiuto M, Deconinck H. A conservative formulation of the multidimensional upwind residual distribution schemes for general nonlinear conservation laws. *Journal of Computational Physics* 2002; **179**: 286–312.
12. Nishikawa H, Rad M, Roe P. A third-order fluctuation-splitting scheme that preserves potential flow. *Fifteenth AIAA Computational Fluid Dynamics Conference*, Anaheim, AIAA Paper 01-2595, 2001.
13. Abgrall R, Barth T. Residual distribution schemes for conservation laws via adaptive quadrature. *SIAM Journal on Scientific Computing* 2002; **24**(3):732–769.
14. Nishikawa H. On grids and solutions from residual minimization. *Ph.D. Thesis*, University of Michigan, Ann Arbor, MI, August 2001.
15. Roe PL. Approximate Riemann solvers, parameter vectors, and difference schemes. *Journal of Computational Physics* 1981; **43**:357–372.
16. Nishikawa H, Rad M, Roe PL. Grids and solutions from residual minimisation. *Computational Fluid Dynamics 2000*. Springer: Berlin, 2000.
17. Roe PL, Nishikawa H. Adaptive grid generation by minimising residuals. *International Journal for Numerical Methods in Fluids* 2002; **40**:121–136.
18. Hirsch C. *Numerical Computation of Internal and External Flows*, vol. 2. Wiley/Interscience: New York, 1990.



DOI: 10.1002/fld